An Interactive Simulation System for Flying Japanese Kites

Taichi Okamoto*
Shizuoka University

Makoto Fujisawa†
Nara Institute of Science and Technology

Kenjiro T. Miura‡
Shizuoka University

(a) Kite festival (b) Various kites (c) Kite simulator (multi-shots)

Figure 1: *Japanese kites and their simulator.*

Abstract

This paper presents an interactive simulation system for flying kites, especially of Japanese types, and discusses the development of a flying kite game with a haptic interface device on a personal computer. The kite interacts with fluid and the computational costs associated with accurate calculation of its behavior are high. The system can precisely calculate the forces induced by air current exerted on the kite based on the graphs of lift and drag coefficients of rectangles with several aspect ratios established by experiments for wings and kites. Hence we can reproduce realistic behaviors of the kite even though it uses a coarse mesh for fluid simulation. The haptic interface device is connected to the simulation system to reflect the drag force applied by the operator and for force feedback from the kite though the kite string to the operator; we have developed a game that gives the feeling of flying a real kite.

CR Categories: I.3.7 [Computer Graphics]: Three-Dimensional Graphics and Realism—Animation; I.6.8 [Simulation and Modeling]: Types of Simulation—Gaming;

Keywords: kite flying, fluid simulation, haptic interface device

*e-mail:f0730024@ipc.shizuoka.ac.jp
†e-mail:fujis@is.naist.jp
‡e-mail:tmkmiur@ipc.shizuoka.ac.jp

1 Introduction

Rapid advances have been made in physical-based simulation techniques in the field of computer graphics for complicated fluid motions and deformations of objects, and the quality of CG animations using these techniques used for cinemas and commercial films is very high, approaching that of video images of real phenomena. Several studies have applied these techniques to hobbies, such as nuigurumi (Japanese rag doll making) [Mori and Igarashi 2007] and origami (Japanese paper folding) [Mitani and Suzuki 2004], which many people enjoy in their daily lives. The goal of our research is to simulate the flying of Japanese kites, a traditional Japanese hobby, as an interactive game. The shapes of the Japanese kites are usually very simple, made up of rectangles or combinations of rectangles. Japanese kites have artistic value because of the traditional paintings on them, as shown in Fig.1(a) and (b).

The kite has a very long history; it was invented more than 2,500 years ago, and fulfilled people's dream of flying before the invention of the airplane. New types of the kite have been developed recently, such as Gayla-kite and bio-kite. Kites are flown at ceremonies and festivals and are used in sports and games. Although kites have long been enjoyed by people, to our knowledge, there have been no previous physical-based interactive simulations of kite flying. This is because the angle of attack can change to a much greater extent than the wing of an airplane and the rigidity of the kite is low and its shape can be deformed easily. Furthermore, it is very difficult to calculate the interactions between a thin plate and airflow even in the field of computational fluid dynamics.

In this paper, we propose an interactive simulation method using the graphs of the lift and drag coefficients of wings and kites established by experiments for performance tests. It is necessary to use a fine grid to accurately calculate the behavior of airflows and the pressure on the upper and lower surface for a thin object using discrete computational methods, such as FDM and FEM, and the computational time tends to be quite long. We obtain the lift and drag coefficients, the working points of the lift and drag forces,

from the shape of the kite and the angle of attack using experimental data. It is not necessary to know the behavior of the airflow around the kite in detail for our method. Hence, we can adopt a coarse-structured grid instead of an unstructured fine grid deformed to the shape of the kite that requires high computational cost. Our fluid simulator calculates the forces exerted by fluid on the kite and obtains the lift and drag forces from their coefficients based on the graphs. The tensile force generated by the kite string is calculated by a mass-spring model and the deformation of the kite is evaluated by assuming that the kite is made of a wireframe. These calculations can be performed in real time.

One of the pleasures of flying kites is to watch their free movement in flight, and another is to control the flight by pulling the kite string, changing the strength and frequency of drag according to the airflow to achieve stable flight. We combined the real-time kite simulator with a haptic interface device to develop a user interactive game. The haptic interface device adds force feedback for input devices and we can control the flight of the kite and give the player the feeling of holding the ends of the kite string. Our ultimate goal is to develop an interactive kite flying game with a haptic interface device.

The goals of our research were to develop the following:

- A fast computation method for the lift and drag forces using experimental data of kites.
- Application of our method for a complicated kite shape by subdividing it into a combination of rectangles.
- A method to control a kite using a haptic interface device.

The rest of this paper consists of the following sections. The following section describes previous work and Sections 3 and 4 address our kite flying simulation techniques and user inteaction. Section 5 shows the results of our simulation. The final section of the paper presents concluding remarks.

2 Related Work

Flying objects other than kites include airplanes and birds. During flight, the air flows around the wing of an airplane and the forces induced by the airflow have been studied in detail [Abbott and Von Doenhoff 1959; Ashley and Landahl 1985; Smith 1992; Wang 2008]. Simulations based on these studies have been performed [Cooke et al. 1992; Bourg 2001]. The aspect ratio of the aerofoil of the airplane is larger than that of a kite, and the maximum angle of attack of the airplane is generally less than $20\,\mathrm{deg}$ although the kite may have larger angles. The delta wing mainly used for military planes has a small aspect ratio and the performance characteristics for relatively large angles of attack have been studied [Regenie et al. 1992; Katz and Plotkin 2004]. However, airplane wings have a certain thickness and are not made of thin material, such as paper or vinyl. The lift force that causes the airplane to elevate has been studied in detail as the airplane flies with thrust force and the drag force against the thrust force is not important for airplane design.

The parawing has been studied for the hang glider [Rogallo et al. 1965; Rogallo 1968]. The specification of the parawing is like a parachute the cloth of which is fixed more loosely than that of the kite.

Ramakrishnananda and Wong [1999] produced bird flight animations based on aerodynamics. They calculated the gravity distribution on the wings of the bird from the wing shape and predicted the flight trajectory based on the aerodynamics. Wu and Popović [2003] modeled a bird as an articulated skeleton with feathers and evaluated the lift and drag forces exerted on the wings by simplified aerodynamics. They used experimental data obtained by Withers [1981] for the lift and the drag coefficients. We adopted simplified aerodynamics similar to those of Wu and Popović [2003] and used experimental data of kites obtained by Azuma [1992] and Ito and Komura [1979].

As a physically-based simulation, fluid dynamics have been used to animate complicated behaviors of water, gas, and flames. In recent years, techniques for animation of complicated interactions between fluid and solid objects have been studied. Stam [1999] proposed a semi-Lagrangian method and a stable and fast fluid calculation method using Fourier domain on a regular cubic mesh, which contributed to improvement of the quality and speed of fluid simulation. Losasso et al. [2004] used an unstructured grid the size of which is finer around free fluid and solid surfaces with less computational cost. However, the boundary regions between the objects and fluid are expressed by hexahedrons and good results are not always obtained. In a study to improve the quality of simulation of fluid-solid interactions using unstructured grids, Feldman et al. [2005] proposed a method to use a regularly hexahedral hybrid mesh but with a tetrahedral mesh around solid objects. Klingner et al. [2006] proposed a method in which a tetrahedral grid is generated according to solid shapes at each time step for interactions with moving solid objects. The generation of tetrahedral meshes requires additional processing time. Guendelman et al. [2005] and Robinson-Mosher et al. [2008] paid attention to thin objects and proposed methods to interact with thin shells. It is very difficult to accurately process interactions with solids in real time.

3 Kite Flying Simulator

In this section, we will describe our kite model and the treatment of the forces exerted to the kite.

3.1 Kite Model

Some kites have artistically complicated shapes and the box kite has a 3-dimensional shape. The kite train consists of several sub-kites, but the kites that can be made at home are rectangular, diamond-shaped, or other simple shapes. We restricted the scope of our discussion to traditional Japanese kites (see, for example, [O-dako]). The traditional Japanese kite has a frame made of bamboo covered with Japanese paper, and is rectangular, diamond-shaped, or yakko, which is a rectangle with sleeves. One or two tails may sometimes be attached at the lower end of the kite to improve the stability of flight. The tails are used to balance the weight on the right and left sides and to stabilize the kite to decrease its angle of attack. Due to the simplicity of its shape, an accurate simulation can be performed based on experimental data for simple shapes.

We use a rectangle of width b and height c as a shape model for the simplest Japanese traditional kite as shown in Fig.2(a). We use a combination of this simple model to treat a kite with a more complicated shape as explained in Section 3.7. Figure 2(b) illustrates the forces exerted on the kite viewed from its side. In addition to the lift and drag forces generated by the airflow around the kite, it has its own gravity, and tensile forces from the kite string and kite tail(s). If the sum of these forces is upward, the kite will fly. The lift and drag forces and their working points have a marked effect on the attitude of the kite, which is determined by rotational motion about the center of gravity of the kite.

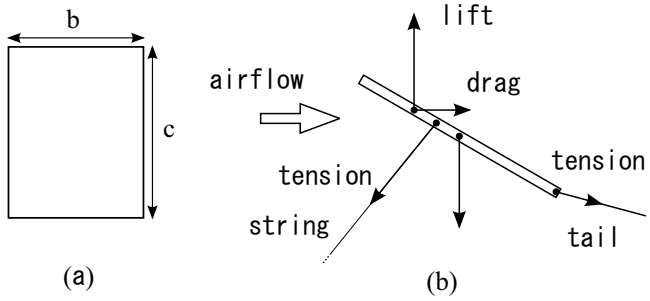

Figure 2: *(a) The basic kite model. (b) Forces exterted on the kite (side view).*

3.2 Lift and Drag Force

The most important factors to determine the kite motion are the lift and the drag forces generated by the airflow. When an aerofoil is placed in the airflow, the airflow velocity becomes different at the upper and the lower surfaces of the aerofoil and the airflow generates a pressure difference. The kite can gain lift force by inclining its attitude and obtain drag force proportional to the projected area on the plane perpendicular to the airflow. It is necessary to know the behavior of the airflow around the kite to calculate the lift and the drag forces accurately. The kite is generally made of paper or vinyl and the simulation between these thin shells and fluid requires a specially shaped grid or FEM. However, these incur high computational costs. For example, Robinson-Mosher et al. [2008] took from several minutes to several hours for the calculation of one frame.

We adopted simplified aerodynamics to obtain the forces exerted on the kite in real time. The lift force $\boldsymbol{L}$ and the drag force $\boldsymbol{D}$ exerted on an object in the fluid are given by:

$$\boldsymbol{L} = \frac{1}{2} C_L \rho S (\boldsymbol{U} \times \boldsymbol{n}) \times \boldsymbol{U}, \quad (1)$$

$$\boldsymbol{D} = \frac{1}{2} C_D \rho S |\boldsymbol{U}| \boldsymbol{U}, \quad (2)$$

where C_L and C_D are the lift and drag coefficients, ρ is the density of air, S is the projected area of the kite, $\boldsymbol{U}$ is the relative velocity of the airflow to the kite, and $\boldsymbol{n}$ is the normal vector of the kite surface. The lift and drag coefficients are determined by the angle of attack, which is the attitude of the kite relative to the airflow. The pressure difference between the upper and lower surfaces of the kite is distributed continuously along the centerline of the kite as illustrated in Fig.3(a). The experimental data obtained by Azuma [1992] substitute this distribution with the resultant force of the lift and drag forces and the working point as shown in Fig.3(b).

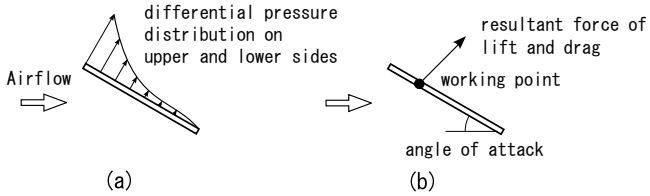

Figure 3: *Force calculation. (a) Differential pressure distribution, (b) Resultant force and its working point.*

We used the three graphs shown in Figs.4-6 in this research, which show graphs of the C_L and C_D to the angle of attack, respectively.

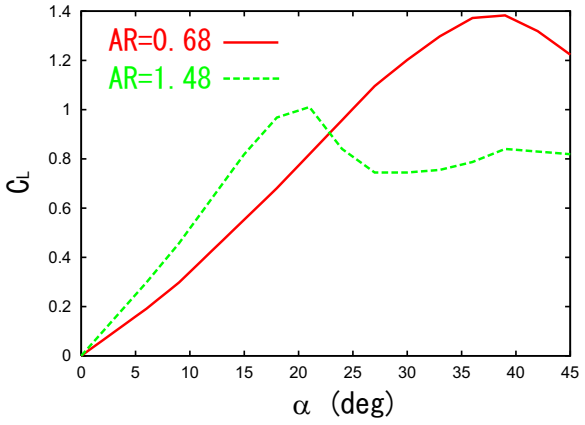

Figure 4: *Variation of C_L with α. $AR = 0.68$(red line) and $AR = 1.48$(green line)*

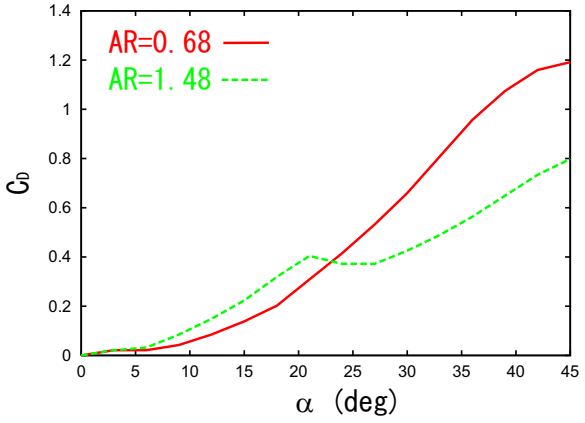

Figure 5: *Variation of C_D with α. $AR = 0.68$(red line) and $AR = 1.48$(green line)*

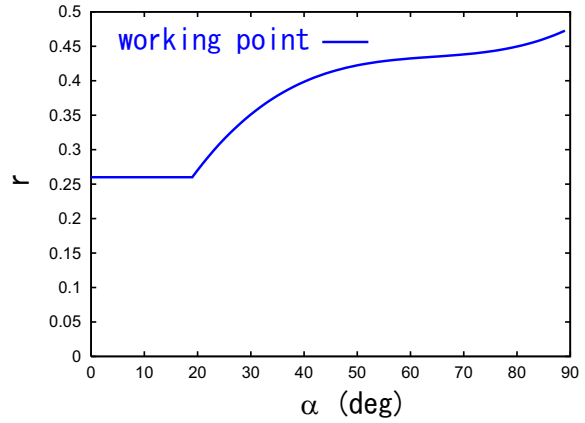

Figure 6: *Variation of r between the front end of the kite to the point of the application of the force/kite height with α.*

The working point of the resultant force of the lift and drag forces is given by the distance rc from the front end to the working point where c is the kite height and the ratio r is obtained by the graph shown in Fig.6 provided by Ito and Komura [1979].

Figures 4 and 5 show the coefficients when the aspect ratios $AR = b/c$ are equivalent to 0.68 and 1.48, respectively. For other aspect ratios, we used a linear interpolation of these data. For $\alpha > 45^\circ$, we use the calculation method for C_L and C_D reported by Wang [2008] given by:

$$C_L(\alpha) = C_L(45^\circ)\sin 2\alpha, \quad (3)$$
$$C_D(\alpha) = C_D(45^\circ)(1-\cos 2\alpha). \quad (4)$$

We obtain the working point exerting the lift force $\boldsymbol{L}$ and the drag force $\boldsymbol{D}$ from Fig.6 [Ito and Komura 1979] for all aspect ratios.

3.3 Lift and Drag Force in 3D

The lift and drag forces are calculated from the pressure distribution along the centerline of the kite. To calculate the motion of the kite in 3-dimensions, we need the pressure distribution on the whole 2-dimensional surface of the kite. However, it is very difficult to estimate the distribution because it depends on the airflow for an object with a complicated shape. As we assumed a rectangular shape for the kite, we expect that the pressure distribution in the direction vertical to the centerline of the kite would be similar to that along the centerline. Here, we established a coordinate system for the kite as shown in Fig.7(a) whose origin is at the center of gravity of the kite. We assumed that the pressure distribution along the x-axis varies with respect to the airflow in the z-x plane in the same manner as that along the y-axis with respect to the airflow in the y-z plane. The pitch motion about the x-axis is calculated from the lift and drag forces and their working point obtained on the plane along the centerline ($x = 0$ plane). Similarly, the roll motion about the y-axis is evaluated by use of the $y = 0$ plane. We use the airflow projected onto the y-z plane to calculate the pitch motion about the x-axis and the airflow projected onto the z-x plane to calculate the roll motion about the y-axis.

For yaw motion about the z-axis, if the kite is assumed to be flat, no lift or drag force is generated. Generally, the kite is deflected by the airflow from the front and generates a force against the yaw motion. This force is necessary to stabilize the attitude of the kite and if it is ignored, the kite will swing right and left continuously. We apply an artificial damping force to stop the yaw motion.

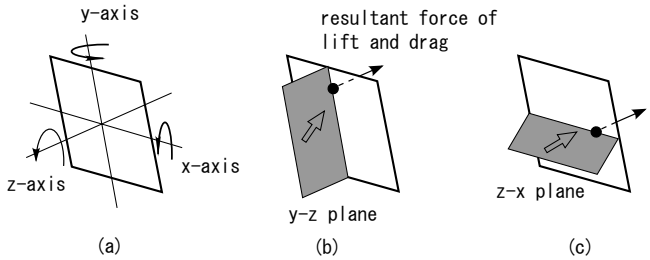

Figure 7: *Extension into 3D. The lift and the drag forces exert along the center line of the 3D kite. We use the airflow projected onto the y-z plane to calculate the pitch motion about the x-axis and the airflow projected onto the z-x plane to calculate the roll motion about the y-axis.*

3.4 Kite String and Tail

One of the tensile forces for the kite is through the kite string controled by the player and the other is by the kite tail which is draged by the airflow. The kite string plays a role of a direct interface with the player and the tail is to balance the right and left weight and to stabilize the kite to decrease its angle of attack. We use a mass-spring model for the kite string and the tail as shown in Fig.8. Each mass is subjected to its gravity, a drag force by the airflow and a tensile force between two connected masses. The drag force is given by Eq.(2). We use a suitable value for C_D by assuming a cylinder or a plane as its shape and S is a projected area of the mass and $\boldsymbol{U}$ is a relative velocity of the airflow to it. The tensile force by the spring $\boldsymbol{F}_{\text{spring}}$ is given by:

$$\boldsymbol{F}_{\text{spring}} = k_s \Delta \boldsymbol{l}_s + k_d \boldsymbol{v}, \quad (5)$$

where k_s is a spring constant, $\Delta \boldsymbol{l}$ is an extension of the spring, k_d is a damping factor and $\boldsymbol{v}$ is a relative velocity of the mass at the end of the spring to that at its start. Furthermore if the mass is connected to the kite with a spring, it get an action force from the kite and the kite get its reaction force. We limit the extension of the kite string and tails by apply the method proposed by Goldenthal et al. [2007] into one dimensional case and shorten the length of the string and those of the tails not to make the simulation of the kite string and tails unrealistic.

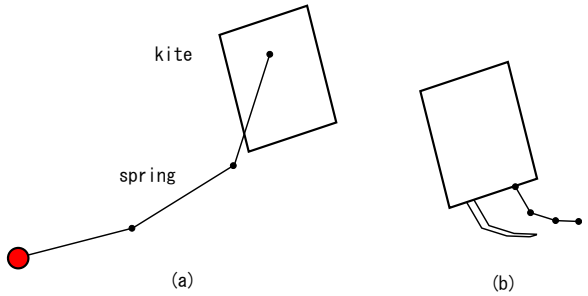

Figure 8: *Mass-spring model of the kite string and the kite tail. (a) String, (b) Tail.*

3.5 Simulation Procedure

The simulation procedure is basically simple and it is similar to those of general physically-based simulations. However, we have steps to limit the extension of the kite string and tails and some special treatment is necessary because the tensions of the string and tails will be decreased very much or become even 0 after their shortening operations.

The simulation procedure is as follows:

```
Initialize kite position, fluid simulator.
Set time interval dt.
Loop:
    Translate the end of the string
       according to the user operation.
    Calculate T_string and T_tail.
    Calculate L and D.
    Calculate force F and moment M
       exerted to the kite.  F is given by:
         F = L + D + G + T_string + T_tail
    Translate and rotate the kite.
    Translate the joints of the string and the
       tails according to the kite motion.
    Shorten the string and the tails.
    Go to Loop.
```

In the above procedure, $\boldsymbol{L}^n$ and $\boldsymbol{D}^n$ are the lift and drag forces at time step n, respectively and $\boldsymbol{G}$ is the gravity of the kite. The tensile force of the kite string to the kite $\boldsymbol{T}^n_{string}$ and that of the tail $\boldsymbol{T}^n_{tail}$ is calculated before the shortening operations. This treatment enables quicker response to the user interaction because the kite string and tails exerts stronger forces to the kite.

3.6 Deflection of Kite

We model the kite as a flat rectangle. The Japanese kite usually uses a bamboo framework, which can be bent easily by a weak force. With deformation of the framework skeleton, the whole kite bends about the y-axis. This deformation improves the stability of the kite. Although the force of restitution is substituted for the damping force, deflection of the kite enhances visual realism. We calculate deflection of the framework along the x-axis to represent deflection of the kite. The deflection d in Fig. 8(a) is given by:

$$d = \frac{P}{48EI}(l - 2x)(l^2 + 2lx - 2x^2), \quad I = \frac{1}{12}ah^3, \quad (6)$$

where P is the tensile force from the kite string, E is the Young's modulus, I is the inertia moment of the wireframe, x is the distance from the y-axis, l is the initial length, and b and h are the width and height, respectively, of the sectional area of the skeleton.

After obtaining d, we scale the kite to keep the initial width of the framework. We calculate the projected length l' as shown in Fig.9(b). S in Eqs. (1) and (2) is given by $S = S_{init}(l'/l)$. The change of S induces the vibration of the kite along the y-axis as a real kite. Because if S is decreased, the lift and drag forces also decrease, then the tensile force of the kite string is weaken and d becomes smaller.

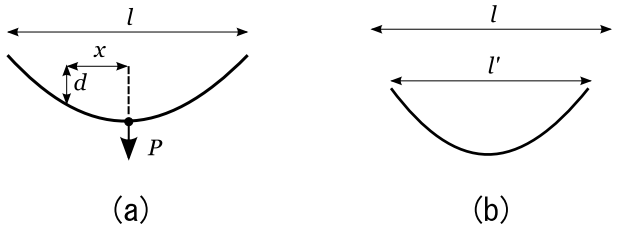

Figure 9: *Kite deflection. (a) Definition of d, (b) Fix the center and calculate the projected length l'.*

3.7 Kite with Complex Shape

We have successfully simulated the motion of a rectangular kite. However, some Japanese kites have a more complex shape. For example, the shape of the yakko can be regarded as a combination of rectangles positioned in parallel with the axes. In this section, we discuss simulation of a kite made of several rectangles.

We assume that the shape of the kite consists of several rectangles. For calculation of the pitch rotation moment, we subdivide the kite into several rectangles each of which has a different height from the adjacent rectangles. For each triangular shape, we calculate the lift and drag forces and the point of force application using the graphs shown in Figs.4-6.

For calculation of the roll rotation moment, we subdivide the kite into several rectangles each of which has a different width from the adjacent rectangles. We calculate the lift and the drag forces and the point of force application in a manner similar to that described for the pitch rotation moment. We sum these forces and moments and obtain the force and moment at and around the center of gravity of the kite.

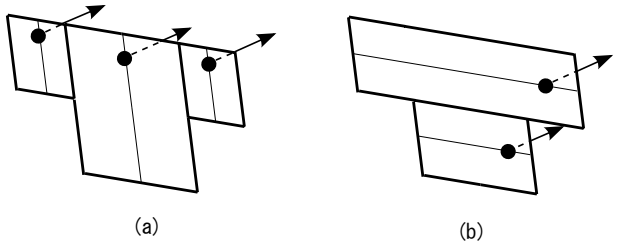

Figure 10: *Complex Shape. (a) We subdivide the kite into several rectangles for each of which has a different width from the adjacent rectangles for the pitch rotation motion. (b) We calculate the lift and drag forces and the working point of the force for roll rotation motion in a manner similar to that described for pitch rotation motion.*

4 User Interaction

The external causes of kite motion are the airflow and kite string operation by the flyer. The behavior of the airflow is controlled by a grid-based fluid simulator and the position of the end point of the kite string assumed to be held by the flyer (red point in Fig.13) is controlled by a haptic interface device with force feedback to enhance the reality of the simulation.

4.1 Fluid Simulation

People fly kites at different locations, e.g., a flat area, a hill top, or a mountainous region under various weather conditions, for example with weak or strong winds, or steady or unsteady winds. We can change the geographical data to emulate different locations and the behavior of the kite naturally becomes dependent on them by use of the fluid simulator.

The governing equations for incompressible viscous fluid are given by:

$$\nabla \cdot \boldsymbol{u} = 0, \quad (7)$$

$$\frac{\partial \boldsymbol{u}}{\partial t} = -(\boldsymbol{u} \cdot \nabla)\boldsymbol{u} - \frac{1}{\rho}\nabla p + \nu \nabla^2 \boldsymbol{u} + \boldsymbol{f}, \quad (8)$$

where ν is the kinematic viscosity and $\boldsymbol{f}$ is the external force, which is the resultant force of gravity and the force exerted by user operation. The above equations are called Navier-Stokes equations. We adopt the method proposed by Stam [1999] to solve Eqs.(7) and (8) and determine the behavior of the airflow. The direction and strength of the airflow are controlled by changing the value of $\boldsymbol{f}$ at certain grid points, for example those on a specified plane. The velocity of the airflow at an arbitrary point is calculated by trilinear interpolation of the eight grid points of the cell that includes the point. The velocity of the airflow $\boldsymbol{u}$ at the connection point between the kite and the kite string is used for $\boldsymbol{U}$ in Eqs.(1) and (2) to calculate the lift and drag forces.

We take into account the effects of swirl and separation of the airflow around the kite using the graphs obtained by experiment. The airflow behind the kite can be assumed to have already passed the kite and does not come back to the kite in a short time and does not directly affect the kite motion. Hence, we neglect any effects from the kite on the airflow in our fluid simulation.

4.2 Kite Manipulation

The user can control the airflow by exerting a force on a certain grid point. However, for kite flying in real situations, the operator pulls the kite string back and forth or right and left to control its flight. The kite string is subjected to a tensile force dragged by the kite and the strength of the force changes depending on the strength of the airflow and the size of the kite. To allow the user to have a feeling similar to real kite string control, we use a haptic interface device that enables 3D input and output. The user can pull the kite string using the haptic interface device and obtain feedback force from the simulator. Both haptic and visual feedback provide an illusion of real kite flying.

The user operation is transferred to the simulator by displacing the position of the end point of the kite string proportional to device displacement. The force exerted on the end of the kite string is transferred to the device operator as $\beta_F \boldsymbol{F}_{\text{spring}}$ where $\boldsymbol{F}_{\text{spring}}$ is in Eq.(5) and β_F is a coefficient that can be changed by the user. By changing β_F, the force feedback by the haptic interface device can be adjusted for users of various ages from children to adults.

5 Results

We have implemented a kite flying simulation system based our method, and present the results of experiments where the user controlled the kite using a haptic interface device.

Figure 11 shows models of rectangular, diamond-shaped, and yakko type kites with textures. The rectangular kite in Fig.11(a) consists of one rectangle and two tails for flying simulation. It has another geometrical model for rendering which consists of 12 $\times$ 12 rectangles to express the effect of the deflection described in Section 3.6. The diamond-shaped kite in Fig.11(b) has two models with a tail to calculate the lift and drag forces. One of them consists of 5 rectangles along the y-axis and the other consists of 5 rectangles along the x-axis for pitching and rolling, respectively. It has the same model for rendering as the rectangular kite and it is smoothed out by mapping the diamond-shaped texture. The yakko kite in Fig.11(c) has two tails and two different models for flying simulation. One of them consists of a single rectangle for its body and another rectangle for each sleeve, for a total of three rectangles for pitching and the other consits of two rectangles for rolling. The yakko kite has the same rendering model as the other kites to express its deflections.

Figure 12 shows differences of the behavior of the kite when we changed the environment for the airflow by fluid simulation. For the kite in Fig.12(a), the air is horizontally flowing from left right and the kite flied stably as the video accompanying this paper shows. On the other hand, the kite in Fig.12(b) flied unstably because the airflow was going upward at the right bottom corner naturally due to the slope inserted in the environment of fluid simulation.

Figure 13 shows the control of the kite by a haptic interface device (Phantom Omni; SensAble Technologies). The operator controls the position of the end point of the kite string and feels the tensile force of the kite string. The kite responses quickly enough to the operator control and when the operator pulls the string, the relative velocity of the airflow increases and the kite receives a stronger lift force. As a result, the kite flies higher just as in the real world.

The processing time including fluid simulation is very fast thanks to the use of experimental data for the lift and drag force calculation and a relatively coarse mesh of 16 $\times$ 16 $\times$ 16 grids and is about 300 fps on a PC with Pentium 4, 3GHz and 2GB memory.

Figure 11: *Typical types of Japanese kites.*

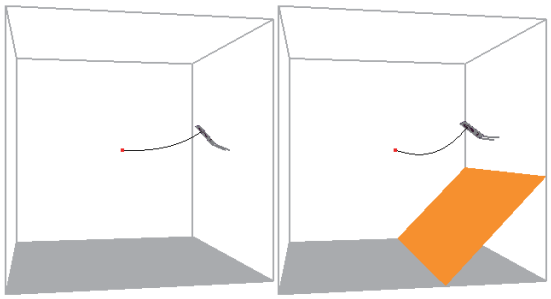

Figure 12: *Different environments.*

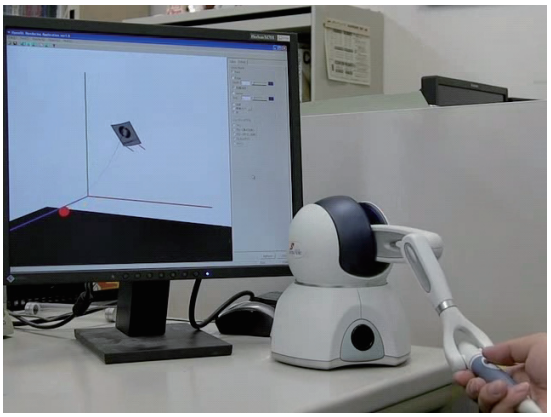

Figure 13: *User interaction.*

6 Conclusions and Future Work

In this paper, we have proposed a real-time kite flying simulation system using the experimental data of the flying kite, a lift and drag force calculation method based on aerodynamics, real-time fluid simulation, and tensile force calculation based on a mass-spring model. Furthermore, we have developed an interactive flying kite game with a haptic interface device. Simulation of the interaction between thin objects and fluid has high computational costs, but we sped up the calculation time by using the experimental data of the coefficients of lift and drag and limiting the interaction to be only from fluid to solid.

We concentrated our efforts on Japanese kites and picked a rectangular kite as the basic type. We have extended our simulation method to be applicable to more complicated shapes by treating them as combinations of rectangles. We took into account the deflection of the kite framework and the kite tails. We could reproduce the changes in the airflow using a computational fluid solver based on the grid caused by the terrain and the differences in altitude.

The data are available for only two different aspect ratios of the rectangle to calculate the coefficients of lift and drag, and we used linear interpolation to calculate them for an arbitrary aspect ratio. For aspect ratios less than 1, the graphs become specific shapes. It is desirable to collect more data, and the interpolation method should be reconsidered in future studies.

As future work, to make our system more enjoyable, we will improve our system to include two or more kites, which will fight with each other; this is called kenka-dako (fighting kites) and will be realized on a computer. Another direction of research is to apply our system to design the shape of the kite and evaluate differences in performance and stability associated with modifications of its shape.

References

ABBOTT, I., AND VON DOENHOFF, A. 1959. *Theory of Wing Sections*. Dover Publications.

ASHLEY, H., AND LANDAHL, M. 1985. *Aerodynamics of Wings and Bodies*. Dover Publications.

AZUMA, A. 1992. *Science of RC Airplane and Kite*. Denpa Jikkensha (Japanese).

BOURG, D. 2001. *Physics for Game Developers*. O'Reilly Media, Inc.

COOKE, J. M., ZYDA, M. J., PRATT, D. R., AND MCGHEE, R. B. 1992. Npsnet: flight simulation dynamic modeling using quaternions. *Presence: Teleoper. Virtual Environ. 1*, 4, 404–420.

FELDMAN, B. E., O'BRIEN, J. F., AND KLINGNER, B. M. 2005. Animating gases with hybrid meshes. In *Proceedings of SIGGRAPH 2005*, ACM Press, New York, NY, USA, 904–909.

GOLDENTHAL, R., HARMON, D., FATTAL, R., BERCOVIER, M., AND GRINSPUN, E. 2007. Efficient simulation of inextensible cloth. In *Proceedings of SIGGRAPH 2007*, ACM Press, New York, NY, USA, 49.

GUENDELMAN, E., SELLE, A., LOSASSO, F., AND FEDKIW, R. 2005. Coupling water and smoke to thin deformable and rigid shells. In *Proceedings of SIGGRAPH 2005*, ACM Press, New York, NY, USA, 973–981.

ITO, T., AND KOMURA, K. 1979. *Science of Kite*. Shogaku-kan (Japanese).

KATZ, J., AND PLOTKIN, A. 2004. Low-speed aerodynamics. *Journal of Fluids Engineering 126*, 293.

KLINGNER, B. M., FELDMAN, B. E., CHENTANEZ, N., AND O'BRIEN, J. F. 2006. Fluid animation with dynamic meshes. In *SIGGRAPH '06: ACM SIGGRAPH 2006 Papers*, ACM, New York, NY, USA, 820–825.

LOSASSO, F., GIBOU, F., AND FEDKIW, R. 2004. Simulating water and smoke with an octree data structure. In *Proceedings of SIGGRAPH 2004*, ACM Press, New York, NY, USA, 457–462.

MITANI, J., AND SUZUKI, H. 2004. Making papercraft toys from meshes using strip-based approximate unfolding. In *SIGGRAPH 2004*, 259–263.

MORI, Y., AND IGARASHI, T. 2007. Plushie: an interactive design system for plush toys. In *SIGGRAPH '07: ACM SIGGRAPH 2007 papers*, ACM, New York, NY, USA, 45.

O-DAKO. Gddweb : Shirone o-dako. http://gddweb.org/odako.html.

RAMAKRISHNANANDA, B., AND WONG, K. C. 1999. Animating bird flight using aerodynamics. *The Visual Computer 15*, 10, 494–508.

REGENIE, V., ET AL. 1992. The f-18 high alpha research vehicle: A high-angle-of-attack testbed aircraft.

ROBINSON-MOSHER, A., SHINAR, T., GRETARSSON, J., SU, J., AND FEDKIW, R. 2008. Two-way coupling of fluids to rigid and deformable solids and shells. In *SIGGRAPH '08: ACM SIGGRAPH 2008 papers*, ACM, New York, NY, USA, 1–9.

ROGALLO, F., SLEEMAN, W., AND CROOM, D. 1965. Resume of recent parawing research. *NASA Technical Reports*.

ROGALLO, F. 1968. Nasa research on flexible wings. *Annals of the New York Academy of Sciences 154*, 2 International Congress on Subsonic Aeronautics, 953–961.

SMITH, H. 1992. *The Illustrated Guide to Aerodynamics*. Tab Books.

STAM, J. 1999. Stable fluids. In *Proceedings of SIGGRAPH 1999*, ACM Press/Addison-Wesley Publishing Co., New York, NY, USA, 121–128.

WANG, Z. 2008. Aerodynamic efficiency of flapping flight: analysis of a two-stroke model. *Journal of Experimental Biology 211*, 2, 234.

WITHERS, P. C. 1981. An aerodynamic analysis of bird wings as fixed aerofoils. *Journal of Experimental Biology 90*, 143–162.

WU, J., AND POPOVIĆ, Z. 2003. Realistic modeling of bird flight animations. In *SIGGRAPH '03: ACM SIGGRAPH 2003 Papers*, ACM, New York, NY, USA, 888–895.